DOI: 10.1002/chem.200701556

Control of Porosity Geometry in Amino Acid Derived Nanoporous Materials

Jorge Perez Barrio,[a] Jean-Noël Rebilly,[a] Benjamin Carter,[a] Darren Bradshaw,[a] John Bacsa,[a] Alexey Y. Ganin,[a] Hyunsoo Park,[a] Abbie Trewin,[a] Ramanathan Vaidhyanathan,[a] Andrew I. Cooper,[a] John E. Warren,[b] and Matthew J. Rosseinsky*[a]

Abstract: Substitution of the pillaring ligand in the homochiral open-framework $[Ni_2(L\text{-asp})_2(bipy)]$ by extended bipy-type ligands leads to a family of layer-structured, homochiral metal-organic frameworks. The 1D channel topology can be modified by the nature of the organic linker, with shape, cross-section and the chemical functionality tuneable. In addition, the volume of these channels can be increased by up to 36% compared to the parent $[Ni_2(L\text{-asp})_2(bipy)]$. The linker 1,4-dipyridylbenzene (3rbp) gives access to a new layered homochiral framework $[Ni_2(L\text{-asp})_2(3rbp)]$ with channels of a different shape. In specific cases, non-porous analogues with the linker also present as a guest can be activated to give porous materials after sublimation. Their CO_2 uptake shows an increase of up to 30% with respect to the parent $[Ni_2(L\text{-asp})_2(bipy)]$ framework.

Keywords: amino acids · chirality · metal–organic frameworks · porous materials

Introduction

The development of materials known as metal-organic frameworks (MOFs) started fifteen years ago.[1–4] The driving interest in this class of compounds was the possibility to synthesize molecular-based solids, whose topology can be controlled by a judicious choice of the building blocks. The introduction of permanent porosity in those materials led to an increasing interest in the discovery of new frameworks that could compete with traditional microporous materials such as zeolites, in various fields of applications, including gas storage, guest separation and catalysis.[5–8] MOF materials have superior sorption capabilities for difficult separations (e.g. *m*- vs. *p*-xylene) to zeolites and can display robust Lewis acid catalytic activity.[9–11]

The development of chiral zeolites remains a difficult task, and the few examples reported have not been applied successfully to stereoselective separation or catalysis.[12,13] Porous homochiral metal-organic frameworks thus appear to be an interesting alternative for such applications. Furthermore, the synthetic strategies in principle allow precise control of the size and functionalities of the pores.

A chiral MOF can crystallize in a chiral space group when prepared from achiral precursors[14] with both enantiomorphs within the bulk sample, leading to a crystalline racemate. The synthesis of homochiral samples requires enantiopure precursors, with chirality located either on the rigid organic spacer connecting metal centers,[15] or in a chiral auxiliary ligand.[16] If an extended chiral component of the structure is robust under the adopted synthetic conditions, it may be possible to access a family of homochiral MOF materials through the choice and design of the organic linker.

Biologically derived chiral ligands are particularly appealing as they are readily available enantiopure, and are inexpensive in the naturally occurring form. Molecules such as lactate[17] and tartrate[18] have already been used for MOF synthesis. The whole class of amino acids, in their L-form, also satisfy the desired criteria. In particular, aspartic acid has been used build homochiral mono-dimensional coordination polymers[19] and a three-dimensional homochiral microporous open framework.[20] We recently reported the synthesis and sorption properties of the chiral open framework

[a] J. Perez Barrio, Dr. J.-N. Rebilly, B. Carter, Dr. D. Bradshaw, Dr. J. Bacsa, Dr. A. Y. Ganin, Dr. H. Park, Dr. A. Trewin, Dr. R. Vaidhyanathan, Prof. A. I. Cooper, Prof. M. J. Rosseinsky
Department of Chemistry, University of Liverpool
Liverpool L69 7ZD (UK)
Fax: (+44) 151-794-3587
E-mail: m.j.rosseinsky@liv.ac.uk

[b] Dr. J. E. Warren
Daresbury Laboratory, Daresbury
Warrington, Cheshire WA4 4 AD (UK)

Supporting information for this article is available on the WWW under http://www.chemeurj.org/ or from the author.

$[Ni_2(L\text{-asp})_2(bipy)]$.[21] The chirality of the pores, induced by the enantiopure amino acid building block, leads to a significant degree of enantioselection in the sorption of a family of small diols with *ee* values up to 54%.

Herein we report the synthesis and characterization of a family of MOFs, derived from the original $[Ni_2(L\text{-asp})_2(bipy)]$ framework, which permits the dimensional tuning and also modification of the pore geometry. Incorporating organic linkers of different shapes and sizes, frameworks with various characteristics such as conformational flexibility or basic functionality within the pores can be obtained.

Results and Discussion

Phases description: Five organic linkers were used to obtain structures derived from the $[Ni_2(L\text{-asp})_2(bipy)]$ framework. Three, 4,4′-azopyridine (azpy),[22] bis(4-pyridyl)ethylene (bpe) and 1,4-bis(4-pyridyl)benzene (3rbp)[23] have the same gross connectivity as 4,4′-bipyridine and can be considered as "extended bipy ligands". The other two, tris(4-pyridyl)-triazine (py_3T)[24] and 3,5-bis(4-pyridyl)pyridine (35bpp)[25] have a different topology and a supplementary pyridyl group (Scheme 1).

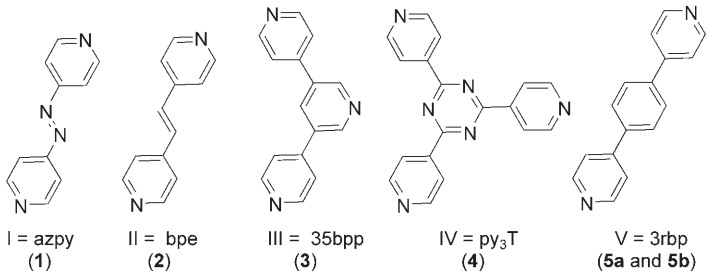

Scheme 1. Scheme of the organic linkers L used in this paper, with accompanying numbering in Roman numerals. The corresponding $[Ni_2(L\text{-asp})_2L]\cdot(guests)$ framework is indicated in bold in brackets.

The reaction of azpy with preformed $[Ni(L\text{-asp})(H_2O)_3]$ under analogous conditions to those used for the synthesis of the original framework leads to a reddish microcrystalline powder of $[Ni_2(L\text{-asp})_2(azpy)]\cdot(guests)$ (**1**). Compound **1** crystallises in the chiral space group $P2_1$ and shows a similar layered structure to that observed in the $[Ni_2(L\text{-asp})_2(bipy)]$ framework.[21] The coordination geometry about each metal centre is a distorted octahedron. Both aspartate molecules act as tridentate ligands, leading to the coordination of the amino group and the oxygen atoms of the α- and β-carboxylate groups to the metal in a *fac* fashion. The nitrogen atom of one pillar ligand is situated in a *trans* position to the amino group of the aspartate molecule. The remaining two coordination sites are occupied by oxygen atoms of carboxylate groups from two adjacent Ni-(asp) entities. This arrangement leads to a corrugated layer in which all Ni centres are surrounded by two α- and two β-carboxylates (Figure 1).

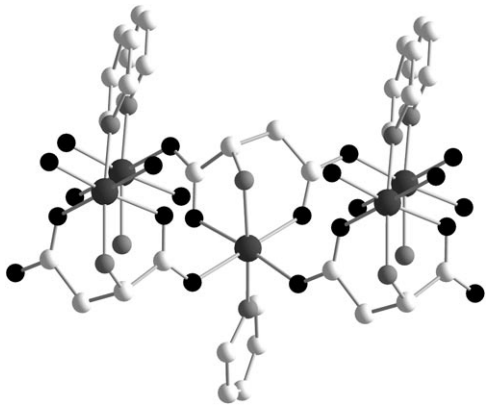

Figure 1. View of the connectivity of aspartate ligands and the arrangement of Ni centres within the [Ni(L-asp)] layer in compound **1**. Ni (dark grey), O (black), C (white), N (medium grey).

Each layer is made from enantiopure ligand, with one L layer connected to an adjacent L layer by the achiral organic linker, leading to an overall chiral crystal (Figure 2). Compound **1** can be thought of as derived from the $[Ni_2(L\text{-asp})_2(bipy)]$ structure by shifting to monoclinic metric symmetry. The Ni(L-asp) layer is built from two independent Ni centres, showing the same overall coordination sphere as in $[Ni_2(L\text{-asp})_2(bipy)]$, but differing in bond lengths and angles.[26] The arrangement of the carboxylates remains the same as in $[Ni_2(L\text{-asp})_2(bipy)]$, with each Ni centre surrounded by two α-carboxylates positioned *trans* to two β-carboxylates. The β angle of the monoclinic cell of **1** is very close to 90°. The *b* parameter can thus be related to the interlayer

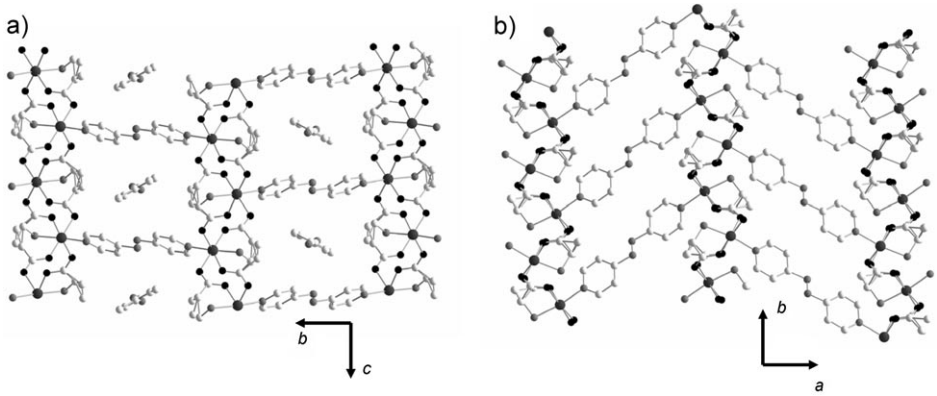

Figure 2. View of the structure of **1**; a) in the (*b*, *c*) plane; b) in the (*a*, *b*) plane (guests omitted). Ni (large, dark grey), O (black), C (grey), N (small, dark grey).

distance and therefore to the size of the linker. In **1**, the longer linker manifests itself by a 2.5 Å expansion along *b* in comparison with the distance in the parent compound. This is in agreement with an increase expected from the insertion of two nitrogen atoms between the pyridine rings of the linker. Another consequence of this length increase is the modification of the topology of the channels in the centre of the host framework. The channels are nearly linear (see Figure S1 in the Supporting Information), non-intersecting but the internal diameters vary between 4.1 × 3.8 Å (windows) and 7.8 × 3.7 Å (pores) in **1**, whereas the channels are sinusoidal with an almost regular cross section (3.8 × 4.7 Å) in the $[Ni_2(L\text{-asp})_2(bipy)]$ framework (all quoted channel dimensions have had the van der Waals radii subtracted). The windows are limited, along the interlayer direction (*b* axis), by the hydrogen atoms of the β-carboxylate group, and along the perpendicular direction (c axis) by the central function of the pillar linker (N=N double bond). The channel dimension along *b* increases from $[Ni_2(L\text{-asp})_2(bipy)]$ to **1** with the length of the pillar linker (from 3.8 to 4.1 Å). In the *c* direction, the distance between two successive azpy ligands varies only by 0.07 Å from $[Ni_2(L\text{-asp})_2(bipy)]$ to **1**. The observed decrease from $[Ni_2(L\text{-asp})_2bipy]$ to **1** of the channel cross-section along *c* (from 4.70 to 3.80 Å) is due to a slight twist of the pyridine rings of the azpy ligand (33.6° for azpy vs. 15.2° for bipy) that projects the nitrogen atoms of the N–N bond further inside the channels. The chiral carbon atom of the aspartate imparts chirality to the internal surface of the channels. The solvent accessible volume per unit cell in **1** is 329.5 $Å^3$, which represents 26.3% of the total cell volume, to be compared to 23.1% in the case of the original bipy framework. This void volume increase is related to the cross section enhancement generated by the azpy ligand with respect to bipy.

The refinements reveal electronic density in the channels that clearly corresponds to disordered azpy molecules. The structural disorder could be modelled accurately using a complete azpy molecule at position $x/a = 1/4$ along the channel axis, while the azpy plane coincides with the diagonal of the *b* and *c* axis, where the windows reach their greatest dimension. But unlike typically incommensurate urea inclusion compounds,[27] the unit cell dimension *a* is commensurate with the repeat unit for the guest along the channel axis (Figure 3a). Although the azpy/host structure is commensurately ordered, the azpy molecule (≈9.5 Å) is 1.5 times longer than the *a*-repeat. If the azpy is ordered within a channel, the natural repeat distance is 9.73 Å. The unit cell that is consistent with the guest repeat is $a \times 1.5 = 9.730$ Å. No extra reflections or diffuse scattering at incommensurate positions were evident from the X-ray diffraction frames, and thus the data were integrated with the smaller cell. As the molecular length of azpy is greater than the *a* axis, the guest molecules are disordered. The structural model that is consistent with the *a*-repeat consists of two overlapping azpy molecules, displaced by an amount that matches the *a*-repeat. This gives the most reasonable structure because the periodicity of neighbouring components matches the *a* axis

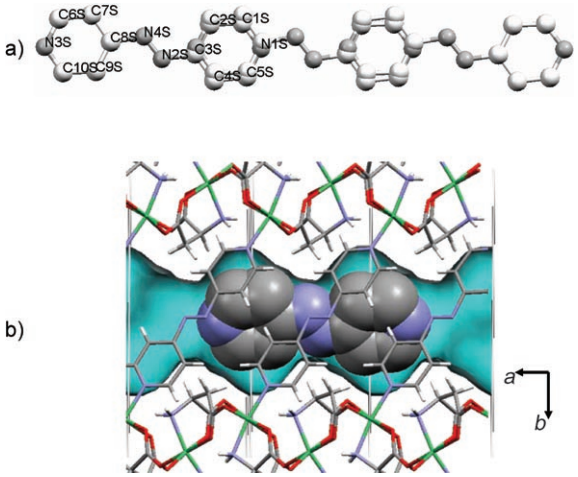

Figure 3. a) A plot of the guest disorder in **1** with overlapping components is shown above. The two disorder components are translated exactly 1 unit-cell repeat from each other along the *a* axis. They occupy favoured positions along the channel axis, so that the narrower -N=N- linkages are non-overlapping and positioned in the narrowest portions of the channels (at approximately $x/a = {}^1/_4$). b) Position of the one guest azpy ligand in the host channels in **1**. Ni (green), O (red), C (grey), N (blue), H (white). (CO_2-excluded surface, calculated for a rolling ball of radius $R = 1.51$ Å) in light blue.

and results in the narrow windows in the structure being occupied by the azo groups only. The azpy ligand (approximate van der Waals dimensions of 12.4 × 6.4 × 3.4 Å) can be inserted in regular channels of 7.8 × 3.7 Å, corresponding to the pore dimensions of **1**. The narrowest portion of the molecule, the central N=N double bond of the linker, with a cross section of 4.1 × 3.1 Å, occupies the narrowest section of the channel (Figure 3b).

The refined population of the azpy molecules in the channels converged to 0.58, in reasonable agreement with elemental analysis considering correlation with the refined parameters. The composition $[Ni_2(L\text{-asp})_2(azpy)](azpy)_{0.6}(H_2O)_{1.4}$ (calcd: C 41.21, H 3.68, N 16.82, Ni 16.78; found: C 41.53, H 3.37, N 16.80, Ni 16.72) determined by elemental analysis confirms the presence of excess ligand in the channels indicated by diffraction.

The powder X-ray diffraction patterns of the bulk samples of **1** were recorded at room temperature and analysed. Le Bail fits of the experimental patterns are in agreement with a pure phase of space group $P2_1$ with room-temperature cell parameters $a = 7.843(4)$, $b = 25.529(15)$, $c = 6.630(4)$ Å, $\beta = 91.516(21)°$ (see Figure S2 in the Supporting Information). The interlayer separation changes significantly from 24.778 Å at 150 K.

The thermogravimetric (TG) curves (see Figure S3 in the Supporting Information) shows a weight loss of 2.9% between 30 and 200 °C, attributed to solvent loss (one water molecule per $[Ni_2(L\text{-asp})_2(azpy)]$ unit) and a second loss of 70.9% between 350 and 800 °C, in agreement with the decomposition of the framework and the guest linkers to NiO and organics (calcd 75.0%). The high decomposition temperature demonstrates the high thermal stability of **1**.

The enantiomeric purity of **1** was checked by GC analysis, with bulk samples possessing enantiomeric excesses for the asp linker of greater than 95%, indicating that the bulk samples are chiral and enantiomerically pure.

In the closely related compound $[Ni_2(L\text{-asp})_2(bpe)]\cdot$(guests) (**2**), made in an analogous manner, the azo group of the bipyridyl pillaring ligand I in **1** is replaced by the -C=C- double bond of ligand II (Scheme 1). Compounds **1** and **2** are isostructural. They both have a slight distortion from the parent orthorhombic structure, and a similar window cross section of 4.1×3.9 Å and pore cross section of 7.8×3.3 Å (see Figure S1 in the Supporting Information). The void volume of **2** represents 24.8% of the total volume.

The phase purity of the bulk samples of **2** was confirmed by powder X-ray diffraction (see Figure S4 in the Supporting Information). Bulk chirality analysis indicates enantiomeric excesses higher than 95%. As in the case of **1**, crystal structure and elemental analysis show the presence of excess bpe ligand in the channels. The electronic density in the channels was modelled as disordered bpe molecules in a similar model to that used for the azpy ligand in **1**. Van der Waals dimensions of bpe are approximately $12.5\times6.4\times3.4$ Å. Pyridyl rings of bpe thus fit in the available pores of dimensions 7.9×3.3 Å. The windows in **2** have a cross section of 4.1×3.9 Å (values along *b* and *c* axis, respectively). The narrowest part of the bpe ligand has a cross section of approximately 4.9×3.4 Å and sits in the windows (see Figure S5 in the Supporting Information). The guests are in an orientation close to Miller planes {012}, when displaced from the origin. The refined population of the bpe in the channels converged to 0.44(1), consistent with that determined by elemental analysis of the bulk sample (elemental analysis leads to the formula $[Ni_2(L\text{-asp})_2(bpe)](bpe)_{0.4}(H_2O)$ for **2**: calcd: C 45.63, H 4.01, N 10.30, Ni 17.98; found: C 45.45, H 3.98, N 10.29, Ni 18.03).

The TG data from **2** (see Figure S6 in the Supporting Information) shows a first weight loss of 2.8% between 30 and 200°C attributed to solvent loss (one H_2O molecule per $[Ni_2(L\text{-asp})_2(bpe)]$ unit) and a second loss of 74.2% due to the decomposition of the framework and guests to NiO and organics (calcd 74.3%). Decomposition occurs between 375°C and 415°C.

The related material $[Ni_2(L\text{-asp})_2(35bpp)]\cdot$(guests) (**3**) is also accessible solvothermally from the linker III (Scheme 1). The connectivity of this ligand is different from those used in the previous two examples as the angle formed by the lone pairs of the terminal pyridines is 120°, not 180°. Compound **3** crystallizes in the chiral space group *C*2 and its overall structure is very similar to that of $[Ni_2(L\text{-asp})_2(bipy)]$ (Figure 4). The 35bpp linker (III) connects Ni(L-asp) layers by its two terminal pyridyl groups. The inner N atom does not coordinate to Ni, but instead forms hydrogen bonds to a neighbouring hydrogen atom of the central aromatic ring of an adjacent 35bpp ligand (Figure 4b). Nevertheless, while the two adjacent Ni(L-asp) layers in the $[Ni_2(L\text{-asp})_2(bipy)]$ framework are related by a 180° rotation about the *c* axis (one of the two-fold axes in $P2_12_12$), they are now related by a 180° rotation about the *b* axis (two-fold axis in *C*2) in compound **3**, a consequence of the different angles formed by the lone pairs in the bipy and 35bpp ligands (Figure 4).

The 35bpp ligand also shows a twist of 31.5° between the central and external pyridines. All the central rings of the 35bpp linkers are aligned along the *b* direction as a result of C–H···N non-classical hydrogen bonding between the pyridyl N atom and the hydrogen atoms of the neighbouring linker (Figure 4b).

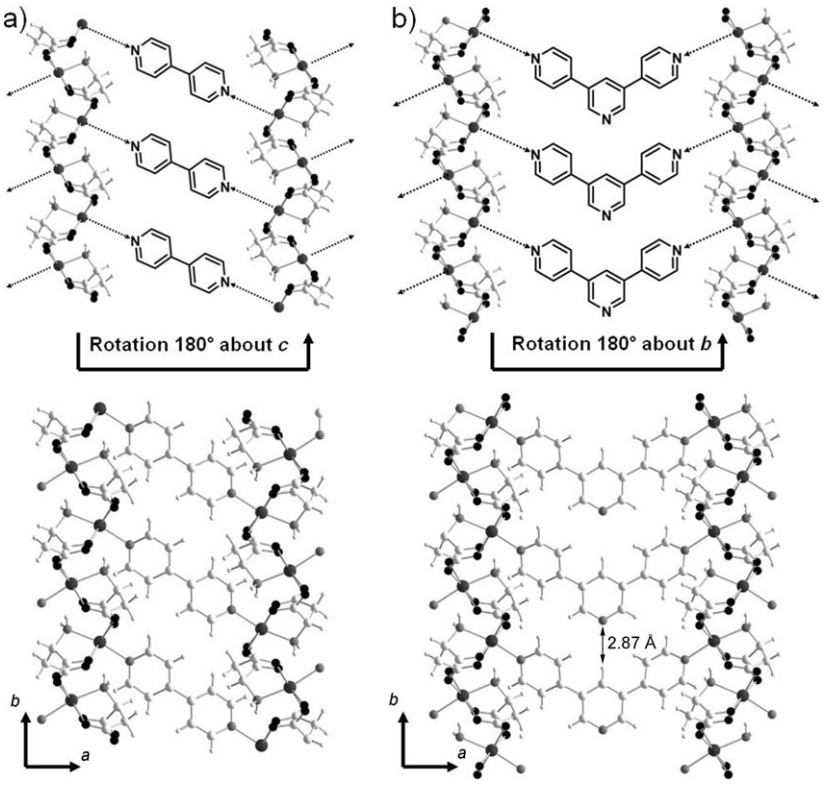

Figure 4. Top: Symmetry relations between the layers in a) $[Ni_2(L\text{-asp})_2(bipy)]$ and b) **3.** The arrows represent the direction of the Ni–N(py) bond. The layers are related by a) a two-fold rotation about *c* in $P2_12_12$; b) A two-fold rotation about *b* in C2. Bottom: Views of the structures of a) $[Ni_2(L\text{-asp})_2(bipy)]$ and b) **3**, showing the N–H interaction between two consecutive 35 bpp linkers (represented in black). Ni (large, dark grey), O (black), C (grey), N (small, dark grey).

This pillared structure gives rise to channels, whose dimensions oscillate between 6.7×4.9 Å and 10.3×5.4 Å (see Figure S1 in the Supporting Information). As in **1** and **2**, there is evidence of the presence of excess 35bpp linker within the channels in the crystal structure. The solvent accessible volume in the host structure in **3** is now 31.4% of the total volume of the framework. The third pyridyl group of the 35bpp ligand is non-coordinating and thus accessible to potential guest molecules. Phase purity of bulk samples was confirmed by LeBail fits of powder X-ray diffraction patterns (see Figure S7 in the Supporting Information) and is in agreement with the phase described above.

Elemental analysis is consistent with the following composition for **3**: $[Ni_2(L\text{-asp})_2(35bpp)](35\ bpp)_{0.333}(H_2O)_{1.333}$ (calcd: C 45.90, H 4.03, N 11.47, Ni 16.02; found: C 45.81, H 3.75, N 11.41, Ni 15.93). This indicates that excess linker is present again. These molecules are located in the channels, as these guest ligands cannot be washed away with methanol. The host framework contains tunnels within which 35bpp molecules (ligand III) could be located. As in the previous structures, these guest molecules display translational disorder along the channel axis. These tunnels (and the 35bpp molecules) are wider than in the previous structures, but the included 35bpp is constrained to form linear extended structures, with space for only one 35bpp molecule in each tunnel segment. The observed electron density corresponding to the translational disorder could be reproduced by starting with a disorder component consisting of a whole 35bpp molecule that when expanded by the space group symmetry resulting in several overlapping guest molecules with a translational component matching that of the *b* axis. The optimal position of the 35bpp along the channel axis was confirmed by translating the ligand as a rigid body along the channel axis and noting the effect on the structure refinement parameters. The position that gave the best results was that with external rings located in the widest sections of the channels (10.3×5.4 Å) and with the middle ring located in the windows of dimensions 6.7×4.9 Å (Figure 5). The modelled guest ligand is flat and its plane almost sits in the *ab* plane. The central ring of the guest interacts by π-stacking with the central rings of 35bpp pillars situated at 3.53 Å along *c* on both sides of the channels. Another interaction occurs between the nitrogen of the central pyridine of the guest and a hydrogen atom of a β-carboxylate of the amino acid backbone at 2.53 Å (Figure 5).

The TG curve of **3** (see Figure S8 in the Supporting Information) shows a weight loss of 4.5% corresponding to loss of one water molecule per $[Ni_2(L\text{-asp})_2(35bpp)]$ unit followed by decomposition to NiO and organics between 380°C and 435°C (calcd: 73.9%, found: 74.2%).

$[Ni_2(L\text{-asp})_2(py_3T)]\cdot(guests)$ (**4**), made from linker IV (Scheme 1), has been obtained as a microcrystalline powder. The space group and cell parameters obtained from small single crystals (see Table S1 in the Supporting Information) allow LeBail fitting of the powder pattern (see Figure S9 in the Supporting Information). The layer cell parameters (a= 7.796(3), b=6.445(2) Å) are typical of the previously observed layered structures and suggest a similar 2D substructure of Ni(L-asp). The product of $c\times\cos(\beta\text{-}90)$ ($a\times\cos(\beta\text{-}90)$ in the case of **3**) represents twice the interlayer distance. This value for **3** and **4** is 30.21 and 29.53 Å, respectively. Such a similarity in interlayer distances suggests that the py_3T linker adopts the same bridging mode as 35bpp, as the lone pairs of the external pyridine groups of py_3T, like 35bpp, form an angle of 120°. Two of the py_3T pyridyl groups are coordinated to two successive layers, whereas the third is not. By analogy with the crystal structure of **3**, for a planar conformation of py_3T, this supplementary pendant pyridyl group would generate steric hindrance with the central ring of the next py_3T ligand in the structure (see Figure S10 in the Supporting Information). To avoid this situation, the ligand has to be slightly bent and the third pyridyl group is expected to be projecting inside the channels.

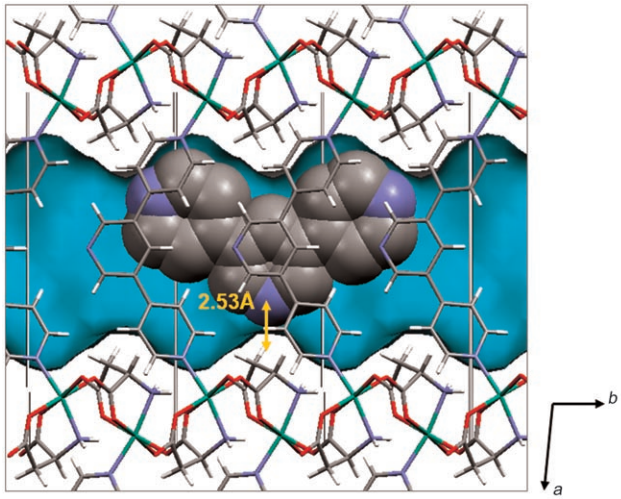

Figure 5. Position of the guest 35bpp ligand in the host channels in **3**. Ni (green), O (red), C (grey), N (blue), H (white). Connolly surface (CO_2-excluded surface, calculated for a rolling ball of radius R=1.51 Å) in light blue. The interaction between the central pyridine of the guest and the H atom of the β carboxylate of the amino acid backbone is represented in yellow.

Elemental analysis and TG analysis (see Figure S11 in the Supporting Information) for **4** is consistent with a framework free of excess linker in the channels. This situation probably arises from their partial occupation by the third pendant pyridyl group of py_3T. The size of the pillar prevents occupation of the channels.

It is noticeable that, in the case of compounds **3** and **4**, despite the presence of three potential coordination sites on the 35bpp and py_3T, only two of them are effectively engaged in coordination to metal atoms leading to the usual layered structure. This indicates that the Ni(L-asp) layer substructure is particularly stable and that its formation is the driving force for building of the whole 3D framework in all of these materials. This is confirmed by the high onset temperature for decomposition (greater than 350°C) in all cases.

Linker V (3rbp) (Scheme 1), as an extended bipy, is expected to lead to a framework that is isostructural to the original $[Ni_2(L\text{-asp})_2(bipy)]$ framework. From powder X-ray diffraction data, the expected isostructural compound **5a** forms as a pure phase (see Figure S10 in the Supporting Information) but cannot be isolated as single crystals. Elemental analysis is consistent with the formula $[Ni_2(L\text{-asp})_2(3rbp)](3rbp)_{0.5}(C_2H_2Cl_4)_{0.25}(H_2O)_{0.75}$: (calcd: C 49.82, H 3.86, N 8.94, Ni 14.98; found: C 49.80, H 3.76, N 9.06, Ni 15.22). Cell parameters extracted from powder data are $a=30.564(2)$, $b=6.812(2)$, $c=7.430(1)$ Å, $\beta=106.680(1)°$ in the space group $P2_1$. The set of parameters b and c suggests the presence of the Ni(L-asp) 2D substructure. The product $a\times\cos(\beta\text{-}90)$ (twice the interlayer spacing) is 29.27 Å, very close to what is observed in **3** and **4** (30.21 and 29.53 Å, respectively) (Figure 6). Elemental analysis shows evidence of the presence of ligands in the channels, as excess ligand can be washed away with tetrachloroethane.

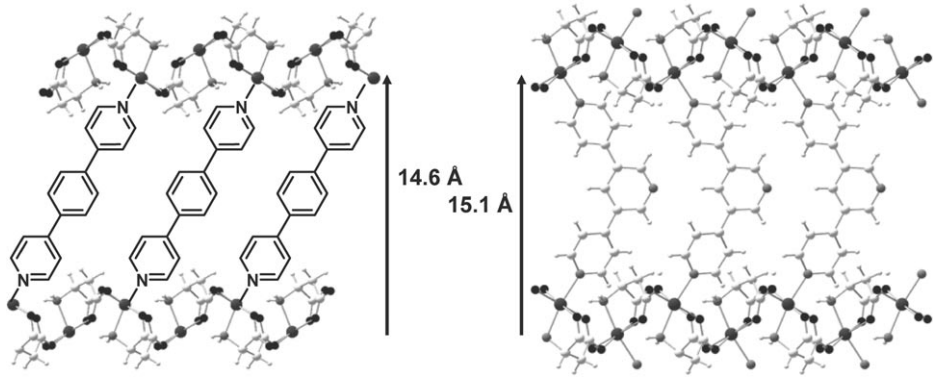

Figure 6. Expected arrangement of 3rbp between the Ni(L-Asp) layers in **5a** (left). Comparison with framework **3** (right). Ni (large, dark grey), O (black), C (grey), N (small, dark grey).

The van der Waals radii of 3rbp are 13.5 Å × 6.2 Å × 3.1 Å for a planar conformation. If the central ring of V is twisted by 45°, the ligand can be included in a box of 13.5 Å × 6.2 Å × 5.1 Å. The expected cross section of the windows, by reference to the original framework, and taking into account the length increase of the ligand, is 8.1 Å × 3.2 Å. The hypothesis of the presence of guest 3rbp in the channels is thus acceptable.

Under modified conditions (smaller volume of 1.5 mL, concentration increased by a factor 5, and reaction time increased to 72 h), a new phase forms from $[Ni(L\text{-asp})(H_2O)_3]$ and 3rbp (ligand V) in a water/1,2-propanediol mixture. Single crystals of this new phase can now be isolated allowing the different structure of **5b** (see Table S1 in the Supporting Information) to be determined, as the characteristic set of parameters related to the Ni(L-asp) substructure are not present here (space group: $P2_12_12$ $a=27.837(15)$, $b=9.892(5)$, $c=10.446(5)$ Å. The overall structure is still layered, but the connectivity of the aspartate ligand is different. The aspartate is tridentate, coordinating in a *fac* fashion and the nitrogen atom of the linker is still *trans* to the nitrogen atom of the aspartate. The difference from $[Ni_2(L\text{-asp})_2(bipy)]$ and compounds **1** to **4** arises from the specific sites occupied in the coordination sphere of nickel by the α- and β-carboxylates. In $[Ni_2(L\text{-asp})_2(bipy)]$ and compounds **1** to **4**, each Ni centre is surrounded by two α- and two β-carboxylates. An α-carboxylate always lies in a *trans* position to a β-carboxylate (Figure 7a).

In compound **5b**, two different Ni centres are present in the unit cell. Ni1 is coordinated to one α- and three β-carboxylates, while Ni2 binds to three α- and one β-carboxylate (Figure 7b). Each Ni1 has thus two coordination sites occupied by the β-carboxylates of one Ni1 and one Ni2 neighbouring centres, whereas Ni2 has two coordination sites occupied by the α-carboxylates of one Ni1 and one Ni2 neighbouring centre. This connectivity generates chains of Ni1 linked by α-carboxylates ("chain 1") and chains of Ni2 linked by β-carboxylates ("chain 2"). The new [Ni(L-asp)] layer is built by bridging alternating chains 1 and 2. One "chain 1" is linked to one "chain 2" by α-carboxylates only and to a second "chain 2" by β-carboxylates only, leading to an irregular arrangement of the aspartate (Figure 7b), whereas α-carboxylates sit in *trans* position to β-carboxylates in a regular fashion in $[Ni_2(L\text{-asp})_2(bipy)]$ (Figure 7a).

The Ni–Ni distances are similar in both cases, with values of 5.515 and 5.332 Å for $[Ni_2(L\text{-asp})_2(bipy)]$ and 5.267, 5.192 and 5.606 Å for **5b**. The Ni-Ni-Ni angles are 90.9 and 79.7° in $[Ni_2(L\text{-asp})_2(bipy)]$, similar to 79.5°, 89.0°, 85.7°, 87.3° and 81.2° for **5b**. Despite those similarities, the different connectivities of the Ni(L-asp) mononuclear units generate two very different Ni(L-asp) layers (Figure 7). In **5b**, two families of linkers are found on either side of the corrugated Ni(L-asp) layer, one connected to the Ni1 centres, the other to the Ni2 centres. Each linker connects a Ni1 centre of one layer to a Ni2 centre of the adjacent layer. Due to the different arrangement of aspartate within these layers, those two families of pillars are not parallel to each other (Figure 8). All the linkers show a twist angle of 44° between the central and external rings of ligand V=3rbp. Channels are nevertheless present but have now an oval form induced by the twist angle between the 3rbp linkers along the b axis. They are far smoother than in frameworks **1**, **2** and **3**, with a cross section oscillating between 6.2 × 4.9 Å and 7.1 × 3.8 Å. This arises from the character of the [Ni(L-asp)] layer itself. The aspartate in this new layer projects the CH_2 group and the oxygen atom of its β-carboxylate outwards inside the channels, leading to a much smoother internal surface. These channels are large enough to incorporate V (=3rbp) molecules. The residual electron density peaks located in the

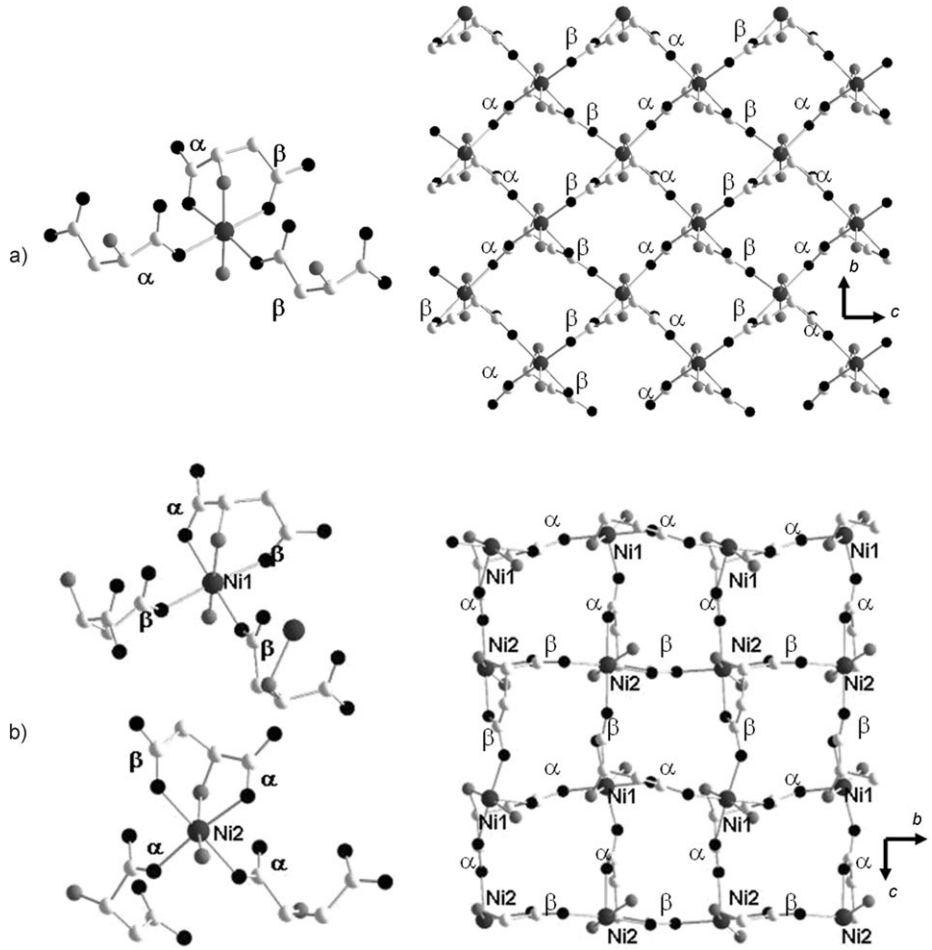

Figure 7. Coordination spheres of Ni centers and their arrangement within the Ni(L-asp) layer in a) [Ni_2(L-asp)$_2$(bipy)]and b) **5b**. Ni (large, dark grey), O (black), C (grey), N (small, dark grey).

channels were assigned as carbon and nitrogen atoms, and without restraints generated an imperfect six-membered ring. A whole 3rbp molecule could be generated by expanding this ring with the point group and translational symmetry of the crystal. The electron density in the channels could be modeled reliably as overlapping whole 3rbp molecules with restraints on the bond lengths and angles (see the Supporting Information). Any section of the 3rbp is now small enough to fit in the windows of the structure due to the less pronounced difference between window and pore dimensions compared to **1**–**4**.

Unlike the azpy, bpe, and 35bpp compounds, the channel ligand components are translated approximately 1 Å from each other, and occupy several positions along the channel axis—it appears that none of these positions are particularly favoured. Again this can be associated with the more regular dimensions of the host channels in **5b**.

Shape and chirality of the channels: A number of general points can be made about the family of frameworks based on the "normal" Ni(L-asp) layer substructure (including **1**, **2**, **3**, **4**, **5a**, and excluding **5b**). For **1**, **2** and **3**, Connolly surface representations revealed the presence of linear channels, with cross section oscillating regularly between window and pore dimensions. This shape has different origins for **1** and **2** on the one hand, and **3** on the other hand. In all cases, the bulky group limiting the channels size in the vicinity of the windows is the CH_2 group of the β-carboxylate of the aspartate backbone. For compound **3**, the 120° angle between the lone pairs of the ligand forces those groups to face each other on both sides of the channels, thus creating windows limited by two of these groups, and a linear shape for the channels, with a cross section oscillating along the channel axis. This situation is expected to occur with any bipy-type ligand showing the same coordination topology as 35bpp (two pyridyl groups which lone pairs form a 120° angle), for instance py_3T. In **1** and **2**, the angle between the lone pairs is 180°, thus, this argument is not valid any more. The length of the ligand plays a significant role here. The distance between two Ni centres connected by azpy (and bpe) is 13.1 Å (bpe: 13.7 Å). Along the *a* axis (channel axis), the projections of those two Ni centres are separated by a distance $L = 6.57$ Å (bpe: $L = 6.83$ Å), which is very close to the cell parameter $a = 6.43$ Å (bpe: 6.48 Å). As a consequence of this match, the CH_2 groups of the β-carboxylate face each other on both sides of the channels, leading to linear channels with a cross section oscillating along the axis (Figure 9a). The chiral centre of aspartate is adjacent to the methylene group that limits the channels, and projects outwards inside them, in the vicinity of their narrow part. The chirality of the channels is thus located in the windows (Figure 9a).

The channel shape is similar for **1** and **2**, and for **3**. In the case of the original framework [Ni_2(L-asp)$_2$(bipy)], the ligand is shorter. The projections, along the channel axis, of the two Ni centres linked by bipy are now separated by $L =$ 5.62 Å, and a mismatch of about 17% with the corresponding cell parameter appears. As a consequence, the CH_2 groups of the β-carboxylates are no longer eclipsed, but staggered, leading to sinusoidal channels (Figure 9b). In compound **5a**, identified from powder data, due to the length of 3rbp, a mismatch of 13% is expected between the

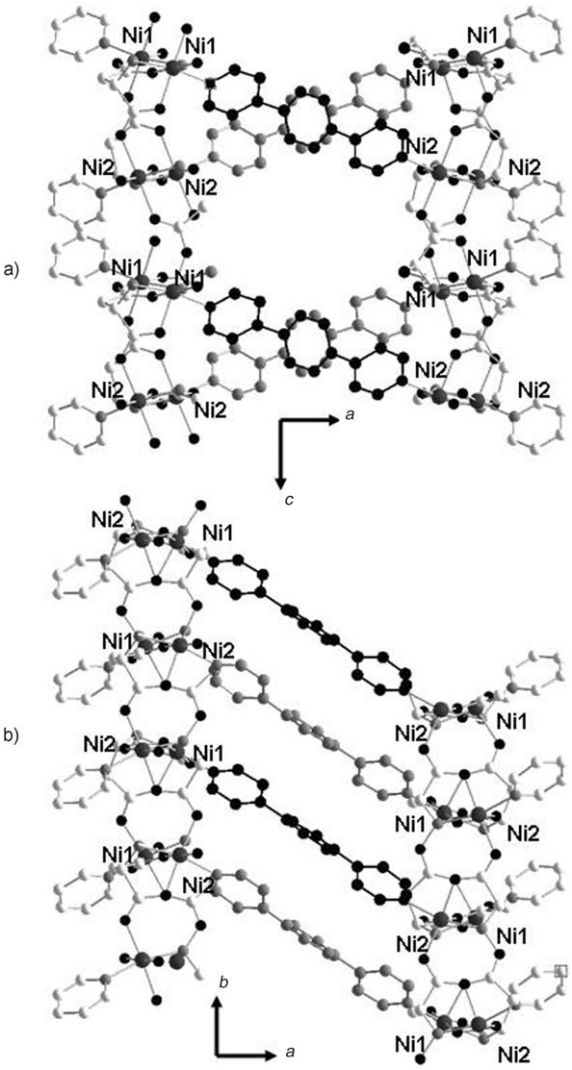

Figure 8. Connectivity of Ni1 and Ni2 in compound **5b**. View along a) the (*a*, *c*) plane; b) the (*a*, *b*) plane. Ni (large, dark grey), O (black), C (grey), N (small, dark grey). The two families of 3rbp pillars are represented in black and medium grey.

cell parameter of the channel axis and the *L* value. Again, sinusoidal shaped channels are probably to be expected in this case. In $[Ni_2(L\text{-asp})_2(bipy)]$, chiral centres are located on both sides of the sinusoidal channels at an average value of $x=0$ on the a axis (channel axis) (Figure 9b). Again, chiral functionality appears on the narrowest part of the channels. The same pattern is expected for **5a**.

In **5b**, the arrangement of the aspartate in the layer is different and gives a smooth character to the surface of the new Ni(L-asp) substructure. This aspect is reflected in the shape of the channels that are also smooth and linear. The formation of two competitive phases **5a** and **5b** with the 3rbp linker, whereas only the "normal" phase is detected with azpy and bpe, probably arises from the match between the shape of the channels and the guest ligand. Compound **5a** is expected to display windows large enough for guest 3rbp to slide along the channels, whereas **5b** shows smooth channels in which 3rbp can move freely. The presence of two families of aspartate ligands in the framework leads to a more regular chiral functionality of the channels. One of the chiral centres manifests itself by narrowing the channels via its C–H bond, whereas the other limits them on their larger section (Figure 9c). The host–guest interactions in **5a** and **5b** must have a similar order of magnitude, justifying the competitive formation of both phases. As previously described, **1** (and **2,** respectively) forms with guest azpy (and bpe, respectively) linker in the channels. The narrowest part of the linker (the -C=C- or -N=N- bonds) sits in the windows, whereas the bulkier pyridyl groups sit in the pores. The guest has no degree of freedom to move along the channels. It is literally trapped in the windows, as channels and guest show almost perfect shape complementarity. In the eventuality of the formation of a competitive phase isostructural to **5b** with the azpy linker, the channels would be smooth. As a consequence, the favourable host–guest complementarity observed in **1** and **2** is probably detrimental to the formation of this hypothetical competitive phase.

The shape of the channels can thus be controlled by the size and topology of the pillar ligand and the solvent mixture. In water/methanol mixtures, a bipyridyl-type ligand with lone pairs forming a 120° angle will lead to linear channels of oscillating cross section (35bpp ligand and framework **3**). Linear bipyridyl linkers can lead either to the same kind of channels, or to sinusoidal channels, depending on their length. Smooth linear channels can also be obtained in competition with the former channels, using linear linkers in water/1,2-propanediol. The channel–guest shape complementarity can then disfavour the formation of those smooth linear channels. This effect is expected to decrease with longer ligands that give rise to wider channels, as larger windows would lose their guest-trapping potential. The interplay between linker geometry, reaction conditions, channel size and guest location in these materials suggests a wide array of pore geometries will be accessible.

Porosity studies: Based on the solvent-accessible volume of these frameworks and the robustness of their backbone, permanent porosity could be expected for compounds **1** to **4**. CO_2 sorption isotherms were thus recorded on those samples. The CO_2 uptake in all cases was below 0.5 mass percent, and the derived BET surface areas were extremely low, confirming the as-made materials are effectively non-porous. For **1** and **2**, the explanation comes from the presence of a large amount of ligand in the channels preventing their access to guest species and gases like CO_2. This is sufficient to block the accessibility of the 1D channels to gas guest molecules, as in a 1D system there is no path around a blockage. Framework **4** is different, with no excess ligand present in the channels; however, the bulky pendant pyridyl group of py_3T projects inside them thus eliminating any porosity. Thus, **4** is *intrinsically* non-porous.

Considering that frameworks **1** to **3** are non-porous due to the presence of excess ligand in the channels, different routes to eliminate these bulky guests and access the frame-

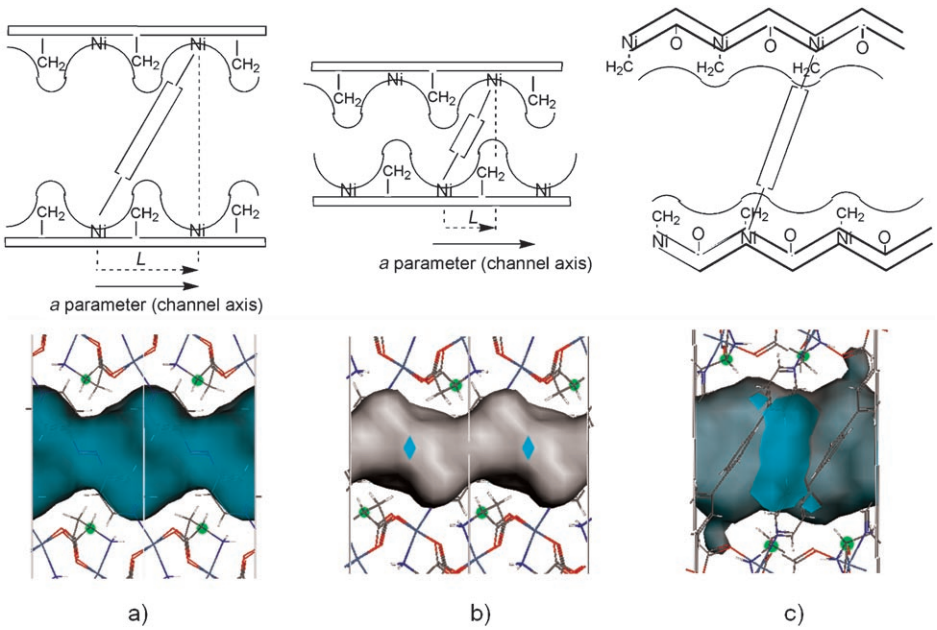

Figure 9. Influence of the ligand size on the shape of the channels. L is the difference between the coordinates (along the channel axis) of two Ni centers connected by the same ligand. a) Case of azpy (framework **1**) (and bpe (framework **2**)). The L value is close to the a parameter. The channels are linear with an oscillating cross section. b) Case of bipy (framework $[Ni_2(L\text{-asp})_2(bipy)]$). There is a mismatch between L and the a parameter. The channels are sinusoidal. c) Case of 3rbp (framework **5b**). The different Ni(L-asp) layer arrangement gives the channels a smoother surface. Lower part: Connolly surface representation (CO_2-excluded surface, calculated for a rolling ball of radius $R=1.51$ Å).

works′ porosity were investigated. For this purpose, several experiments, based on solid–liquid extraction (in a variety of refluxing solvents, or continuous Soxhlet extraction), or on the use of a substitute template guest (co-solvent like toluene or pyridine) were carried out, all proving unsuccessful. Organic molecules have been reported to be removed from porous MOFs under vacuum conditions.[28] We removed the guest ligand molecules by sublimation under dynamic high-vacuum conditions (10^{-4} Torr) at 210°C (see paragraph II and Figure S13 in the Supporting Information).

An accurate heating period is crucial for the total removal of the ligand; if sublimation is incomplete, small amounts of guest ligand can still be present, blocking the 1D channels, keeping the material non-porous.

In the case of **1**, the cooling rate appears to be very important, as it can favour the formation of different post-sublimation phases, which were identified and characterised by powder X-ray diffraction. If the cooling rate is fast ($190\,°C\,min^{-1}$), a first pure single phase $\mathbf{1}_{fc}$ is obtained (see Figure S14 in the Supporting Information), whereas if the cooling rate is slow ($1\,°C\,min^{-1}$), another phase forms alongside $\mathbf{1}_{fc}$.

Elemental analysis of $\mathbf{1}_{fc}$ is consistent with a framework free of guest molecules ($[Ni(L\text{-asp})(azpy)_{1/2}]\cdot(H_2O)_{0.5}$, (calcd: C 37.29, H 3.13, N 14.50; found: C 37.10, H 3.30, N 14.78)). A LeBail fit of $\mathbf{1}_{fc}$ allows us to extract the following cell parameters $P2_12_12$, $a=7.778(1)$, $b=26.173(3)$, $c=6.651(1)$ Å (see Figure S14 in the Supporting Information). Those parameters suggest the presence of the Ni-(L-asp) substructure already present in the as-made material (the a and c parameters have the typical values expected for this substructure) and a larger interlayer spacing as documented by the increase in the b parameter, from 24.77(15) to 26.173(3) Å. This increase can be understood by the specific torsion ability of the pillaring ligand. Depending on the arrangement of azpy molecules between the layers, two extreme "conformer structures" are possible (Figure 10).

A transition from ′conformer 1′ to ′conformer 2′ would be possible without breaking the framework via a simultaneous 180° torsion of all azpy linkers. This transition would lead to an estimated increase of the interlayer distance by 0.95 Å, and an increase of the b parameter by approximately 1.9 Å. The expansion of the b parameter observed in $\mathbf{1}_{fc}$ is thus in

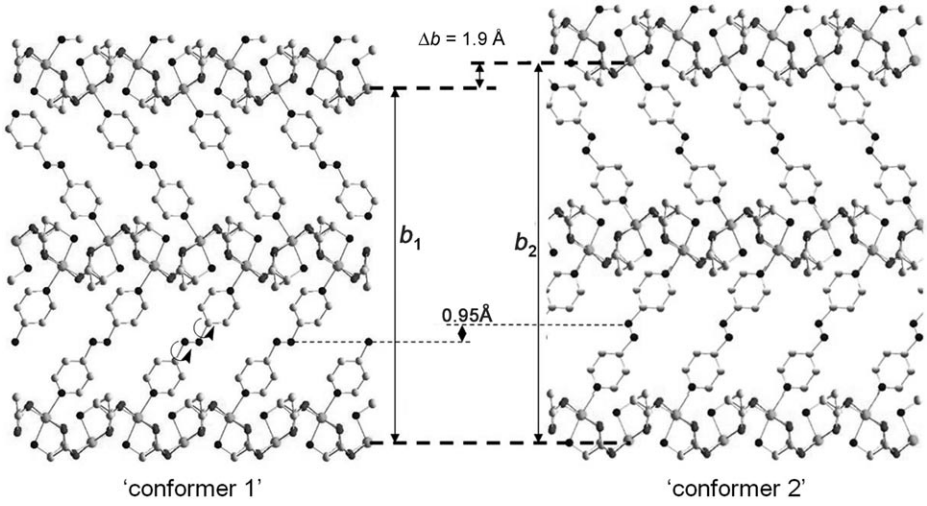

Figure 10. Scheme of the two extreme "conformer structures" potentially accessible to $[Ni_2(L\text{-asp})_2(azpy)]$ via simultaneous torsion of all azpy ligands. Ni (large, dark grey), O (black), C (grey), N (small, dark grey).

an accessible. The CO_2 sorption isotherm(s) of the sublimed phase $\mathbf{1_{fc}}$ was recorded at 198 K (Figure 11). The as-made material is non-porous to CO_2 with an uptake of 0.5%,

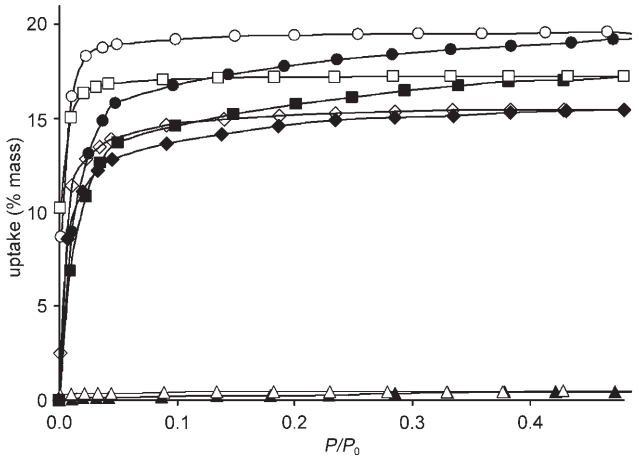

Figure 11. CO_2 sorption isotherms at 198 K. As-made material **1** (triangle), original $[Ni_2(asp)_2(bipy)]$ framework (rhombus), and $\mathbf{1_{fc}}$ (ring). (Adsorption: plain, desorption: empty).

whereas the sublimed phase is porous with a CO_2 uptake of 19.4% for the $\mathbf{1_{fc}}$ phase, leading to a derived BET surface area of 297(6) m^2g^{-1}. This represents an enhancement of the gas uptake of up to 30% with respect to the original framework (15% CO_2 uptake, BET surface area of 243 m^2g^{-1}), due to the increase in the size of the pillaring ligand. Sublimation under high vacuum thus restores the framework's porosity.

Phase $\mathbf{1_{fc}}$ is obtained in a pure form under high vacuum and fast cooling conditions. Under slow cooling conditions, a competitive phase forms, showing that $\mathbf{1_{fc}}$ is favoured under high vacuum and high temperature (sublimation conditions) and trapped by the fast cooling process. This provides insight in the mechanism of azpy sublimation. In the as-made material **1**, we demonstrated that the guest azpy was trapped in the windows of the channels and unable to slide along them. To remove those guests, an expansion of the channels is necessary. Transition from "conformer 1" to "conformer 2" would lead to a 0.95 Å increase in the interlayer spacing and thus of the channel cross section, and would modify the shape of the channels. The estimated value of the parameter *L*, as defined in Figure 9, would be around 5 Å now, leading to a mismatch with the channel axis parameter of 25%. As in the case of $[Ni_2(L\text{-}asp)_2(bipy)]$, channels are expected to be sinusoidal. The guest would then regain the ability to move along the channels, as the windows are no longer able to trap it. This hypothesis for the sublimation mechanism is corroborated by the interlayer spacing increase observed in $\mathbf{1_{fc}}$. Indeed, the cell parameters of this high vacuum trapped phase suggest a situation close to the one of "conformer 2", which could be favoured under sublimation conditions.

Carbon dioxide sorption isotherms based on the structure of $[Ni_2(L\text{-}asp)_2(azpy)]$ were calculated at 198 K using the sorption module of software Materials Studio Modeling 4.0. For this purpose, guests were deleted from the structure of **1** to evaluate the sorption properties of the host. The simulation predicts a CO_2 uptake of 9.2% at 0.76 bar, much lower than the experimental value of 19.7% obtained for $\mathbf{1_{fc}}$. This can be explained by the structural difference between the host in **1** and the host in the sublimed phase $\mathbf{1_{fc}}$. Indeed, **1** is close to what we described as "conformer 1", whereas powder data for $\mathbf{1_{fc}}$ suggests a situation closer to "conformer 2" (Figure 10). The simulated CO_2 density is located in the pores of the structure and absent from the windows. In $\mathbf{1_{fc}}$ (by reference to "conformer 2"), channels are expected to be wider and more sinusoidal, allowing carbon dioxide to occupy a greater space along the channels.

When scaled with a factor $\Phi = 2.25$, the simulation reproduces very well the shape of the experimental sorption (see Figure S15 in the Supporting Information). Scale factors have already been used to take into account occluded pores.[29,30]

A similar behaviour is observed for compound **2**, built from bpe, as torsion of the ligand is possible as in azpy. Nevertheless, the high vacuum and high temperature phase cannot be isolated as a single phase.

The difference in the interlayer spacing between the as-made (**1**) and the sublimed ($\mathbf{1_{fc}}$) phases suggests a certain degree of flexibility and guest-responsive behaviour for compounds **1** or **2**. This has been observed with several compounds[31–34] including bpe and azpy based frameworks.[35] The same sublimation procedure applied to compound **3** was unsuccessful and led to a deterioration of the framework as shown by the broadening of the powder pattern reflections.

In the as-made materials, the guest molecules are "trapped" in the window section of the channels (Figure 3b, Figure S5 in the Supporting Information and Figure 5). To be able to remove them by sublimation, the host framework has to be flexible enough to allow an expansion of the window size to the point where the guest can move along the channels, without hindrance. This is possible in the case of **1** and **2**, thanks to the torsion ability of the azpy and bpe ligands (for **1**, torsion of azpy can lead to an increase of the interlayer spacing of up to 0.95 Å and to a window cross section of up to 5.1×3.9 Å , making the release of the guest possible). This phenomenon is absent in **3**, due to the rigid character of 35 bpp. Sublimation can only lead to a degradation of the framework.

Conclusion

Amine-pillared metal aspartates are a tuneable family of chiral porous materials for which the channel dimensions can be varied through both linker changes and modification of synthetic conditions to produce chiral channels capable of accommodating six-membered rings. As often observed in porous metal–organic frameworks synthesis, porosity is avoided by guest inclusion in the present case, the guest

being the pillar ligand itself. Thanks to the high stability of the layered structures of those frameworks, sublimation of the guests under high vacuum enables restoration of their porosity. Using pillaring ligands including double bonds as a spacing group, sublimation can lead to porous frameworks. The modification of the interlayer spacing due to linker conformational change, depending on temperature and pressure conditions and on the presence of guest molecules, suggests that the channel dimensions could respond selectively and specifically to guest molecules. The original $[Ni_2(L\text{-asp})_2(bipy)]$ showed remarkable enantioselection for a family of small diols, but the dimensions of the channels were the limiting factor for the sorption of larger chiral molecules. The new porous materials reported here can thus be expected to be enantioselective for a wide range of molecules as the framework is stable in two different porous forms. The other striking aspect of these tunable systems is the possibility to introduce functionalities within the pores via the organic linker. The 35bpp system (compound **3**) illustrates the possibility to introduce a basic active site inside the pores. The general approach of robust structural units linked by chiral biologically derived ligands and modifiable organic pillars thus appears promising for the systematisation of chiral open frameworks.

Experimental Section

Single crystal X-ray diffraction: The single-crystal diffraction data were collected on stations 9.8 and 16.2SMX of the Synchrotron Radiation Source at Daresbury Laboratory. Station 16.2SMX and station 9.8 are high flux single crystal facility which utilise a Bruker-Nonius APEXII CCD area detector and D8 diffractometer at an X-ray wavelength of 0.8184 Å (**1**), 0.6727 Å (**2**), 0.7848 Å (**3**), 0.6904 Å (**4** and **5b**) on station s 16.2SMX and 9.8. Data was recorded at 150 K.

Thermal analysis: TGA data were recorded using a Seiko S-II instrument.

Chiral GC analysis: determination of the bulk chirality of the frameworks: Firstly, the aspartic acid needs to be extracted from the bulk material, and is done so by adding 1N NaOH (4 mL) to the framework (30 mg) and removing the resulting precipitate by filtration through a small plug of cotton wool. The addition of NaOH results in the precipitation of insoluble $Ni(OH)_2$ and the organic linker, also insoluble in basic aqueous solution. Removal of the solids leaves the disodium aspartate in the filtrate. It is neutralised by addition of 1N HCl and evaporated to dryness in vacuo. The resulting white solid is a mixture of aspartic acid and NaCl. The aspartic acid is then derivatised prior to GC analysis. The carboxylic acid groups are converted to methyl esters by refluxing in MeOH (4 mL) and HCl (4N, 1 mL) for 4 h. The primary amine is transformed into an amide by reaction with TFA (0.5 mL in 5 mL CH_2Cl_2, room temperature, overnight). The crude mixture is filtered to remove NaCl and the filtrate containing only Asp(OMe/TFA) is evaporated to dryness.The concentration for GC analysis is 0.5% (w/v) Asp(OMe/TFA) in CH_2Cl_2 and is carried out using a Lipodex-E capillary-GC column at 120°C.

X-ray powder diffraction: X-ray powder diffraction data were collected with $Cu_{K\alpha 1}$ radiation with a Stoe Stadi-P diffractometer using a linear position sensitive detector and with $Co_{K\alpha 1}$ radiation with a Panalytical X′pert Pro Multi-Purpose diffractometer.

Sorption isotherm measurements: CO_2 sorption isotherms were measured using a Hiden IGA gravimetric sorption balance at 198 K. Prior activation of samples was carried out at 120°C overnight.

Synthesis: 4,4′-azopyridine (azpy),[22] 1,4-bis-(4-pyridyl)-benzene (3rbp),[23] tris-(4-pyridyl)-triazine (py_3T)[24] and 3,5-bis-(4-pyridyl)-pyridine (35bpp)[25] were prepared according to literature methods. Bis(4-pyridyl)ethylene (bpe) was purchased from Aldrich.

$[Ni_2(L\text{-asp})_2(azpy)](azpy)_{0.6}(H_2O)_{1.4}$ (1): $[Ni(L\text{-asp})(H_2O)_3]$ (0.1 g, 0.4 mmol) and azpy (0.075 g, 0.8 mmol) were added to a water/methanol mixture (4 mL/2 mL) in a 23-mL teflon liner and allowed to react under solvothermal conditions at 150°C for 48 h. Initial pH 7.6. The crude product was filtered and washed thoroughly with methanol, giving red microcrystals. Yield: 70%. Elemental analysis calcd (%) for $[Ni_2(L\text{-asp})_2(azpy)](azpy)_{0.6}(H_2O)_{1.4}$ (699.4): C 41.21, H 3.68, N 16.82, Ni 16.78; found: C 41.53, H 3.37, N 16.80, Ni 16.72.

$[Ni_2(L\text{-asp})_2(bpe)](bpe)_{0.4}(H_2O)$ (2): $[Ni(L\text{-asp})(H_2O)_3]$ (0.1 g, 0.4 mmol) and bpe (0.074 g, 0.8 mmol) were added to a water/methanol mixture (4 mL/2 mL) in a 23-mL teflon liner and allowed to react under solvothermal conditions at 150°C for 48 h. Initial pH 7.2. The crude product was filtered and washed thoroughly with methanol, giving green microcrystals. Yield: 65%. Elemental analysis calcd (%) for $[Ni_2(L\text{-asp})_2(bpe)](bpe)_{0.4}(H_2O)$ (652.6): C 45.63, H 4.01, N 10.30, Ni 17.98; found: C 45.45, H 3.98, N 10.29, Ni 18.03.

$[Ni_2(L\text{-asp})_2(35bpp)](35bpp)_{1/3}(H_2O)_{1.33}$ (3): $[Ni(L\text{-asp})(H_2O)_3]$ (0.1 g, 0.4 mmol) and 3,5-DPP (0.11 g, 0.47 mmol) were added to a water/methanol mixture (2 mL/4 mL) in a 23-mL teflon liner and allowed to react under solvothermal conditions at 150°C for 48 h. Initial pH 7.2. The product was filtered, washed with methanol and isolated as light green crystals. Yield: 67%. Elemental analysis calcd (%) for $[Ni_2(L\text{-asp})_2(35bpp)](35bpp)_{1/3}(H_2O)_{1.33}$ (732.6): C 45.90, H 4.03, N 11.47, Ni 16.02; found: C 45.81, H 3.75, N 11.41, Ni 15.93. Measured bulk chirality *ee*: 70%.

$[Ni_2(L\text{-asp})_2(py_3T)](H_2O)_{0.5}$ (4): $[Ni(L\text{-asp})(H_2O)_3]$ (0.1 g, 0.4 mmol) and py_3T (0.128 g, 0.4 mmol) were added to a water/methanol mixture (3 mL/3 mL) in a 23-mL teflon liner and allowed to react under solvothermal conditions at 150°C for 48 h. The crude product was filtered and the excess ligand dissolved in hot dichloromethane. A second filtration gives the product as green microcrystals. Yield: 66%. Elemental analysis calcd (%) for $[Ni_2(L\text{-asp})_2(py_3T)](H_2O)_{0.5}$ (701.0): C 44.55, H 3.30, N 15.98, Ni 16.75; found: C 44.24, H 3.12, N 15.90, Ni 16.67. Measured bulk chirality *ee*: 66%.

$[Ni_2(L\text{-asp})_2(3rbp)](3rbp)_{0.5}(C_2H_2Cl_4)_{0.25}(H_2O)_{0.75}$ (5a): $[Ni(L\text{-asp})(H_2O)_3]$ (0.031 g, 0.13 mmol) and 3rbp (0.028 g, 0.13 mmol) were added to a water/methanol mixture (3 mL/1 mL) in a 23-mL teflon liner and allowed to react under solvothermal conditions at 150°C for 48 h. Initial pH 7.11. The product was filtered, washed with hot tetrachloroethane and isolated as light green microcrystals. Yield: 66%. Elemental analysis calcd (%) for $[Ni_2(L\text{-asp})_2(3rbp)](3rbp)_{0.5}(C_2H_2Cl_4)_{0.25}(H_2O)_{0.75}$ (783.4): C 49.82, H 3.86, N 8.94, Ni 14.98; found: C 49.80, H 3.76, N 9.06, Ni 15.22.

$[Ni_2(L\text{-asp})_2(3rbp)](3rbp)_{0.5}$ (5b): $[Ni(L\text{-asp})(H_2O)_3]$ (0.062 g, 0.26 mmol) and 3rbp (0.056 g, 0.26 mmol) were added to a water/1,2-propanediol mixture (1.125 mL/0.375 mL) in a 23-mL teflon liner and allowed to react under solvothermal conditions at 150°C for 72 h. Light green single crystals suitable for X-ray diffraction were isolated.

Crystal data: CCDC-662393 (compound **5b**), CCDC-662394 (compound **3**), CCDC-662395 (compound **1**), CCDC-662396 (compound **2**) contain the supplementary crystallographic data for this paper. These data can be obtained free of charge from The Cambridge Crystallographic Data Centre via www.ccdc.cam.ac.uk/data_request/cif.

Crystal data for $[Ni_2(L\text{-asp})_2(azpy)](azpy)_{0.6}(H_2O)_{1.4}$: $C_{23}H_{24.8}N_8Ni_2O_{9.4}$, $M=699.55$, green prism, $0.02\times0.01\times0.01$ mm^3, monoclinic, space group $P2_1$ (no. 4), $a=6.487(4)$, $b=24.779(15)$, $c=7.805(5)$ Å, $\beta=91.029(6)°$, $V=1254.3(13)$ Å^3, $Z=2$, $\rho_{calcd}=1.852$ g cm^{-3}, $F_{000}=719$, Bruker D8 diffractometer, synchrotron radiation, $\lambda=0.8184$ Å, $T=150(2$ K, $2\theta_{max}=50.8°$, 5964 reflections collected, 3128 unique ($R_{int}=0.0912$). Final $GooF=1.037$, $R1=0.105$, $wR2=0.233$, R indices based on 1955 reflections with $I>2\,\sigma(I)$ (refinement on F^2), 234 parameters, 240 restraints. Lp and absorption corrections applied, $\mu=1.579$ mm^{-1}. Absolute structure parameter $=0.12(10)$.

Crystal data for [Ni_2(L-asp)$_2$(bpe)](bpe)$_{0.4}$(H_2O): $C_{28}H_{25.33}N_6Ni_2O_{9.33}$, M = 712.62, green plate, 0.02×0.01×0.004 mm3, monoclinic, space group $P2_1$ (no. 4), a = 6.429(4), b = 25.180(15), c = 7.874(5) Å, β = 90.101(7)°, V = 1274.6(13) Å^3, Z = 2, ρ_{calcd} = 1.583 g cm^{-3}, F_{000} = 624, Bruker D8 diffractometer, synchrotron radiation, λ = 0.6727 Å, T = 150(2 K, $2\theta_{max}$ = 61.0°, 10403 reflections collected, 6843 unique (R_{int} = 0.0468). Final *GooF* = 1.055, *R1* = 0.0906, *wR2* = 0.2352, *R* indices based on 5110 reflections with $I > 2\sigma(I)$ (refinement on F^2), 261 parameters, 318 restraints. Lp and absorption corrections applied, μ = 1.532 mm^{-1}. Refined with TWIN −1 0 0 0 −1 0 0 0 1 −4. The refined twin population parameters (BASF) were 0.25355 0.13160 0.16115.

Crystal data for [Ni_2(L-asp)$_2$(35bpp)](35bpp)$_{1/3}$(H_2O)$_{1.33}$: $C_{23}H_{21}N_5Ni_2O_8$, M = 712.62, green prism, 0.10×0.03×0.02 mm3, monoclinic, space group $C2$ (no. 5), a = 30.840(15), b = 6.574(3), c = 7.704(4) Å, β = 101.557(6)°, V = 1530.4(13) Å^3, Z = 2, ρ_{calcd} = 1.546 g cm^{-3}, F_{000} = 732, Bruker D8 diffractometer with APEXII detector, synchrotron radiation, λ = 0.7848 Å, T = 150(2 K, $2\theta_{max}$ = 51.4°, 3839 reflections collected, 2525 unique (R_{int} = 0.0635). Final *GooF* = 1.077, *R1* = 0.0790, *wR2* = 0.2027, *R* indices based on 2145 reflections with $I > 2\sigma(I)$ (refinement on F^2), 181 parameters, 1 restraint. Lp and absorption corrections applied, μ = 1.278 mm^{-1}. Absolute structure parameter = −0.01(5).

Crystal data for [Ni_2(L-asp)$_2$(3rbp)](3rbp)$_{0.5}$: $C_{32}H_{28}N_5Ni_2O_8$, M = 728.01, green prism, 0.10×0.02×0.01 mm^3, orthorhombic, space group $P2_12_12$ (no. 18), a = 27.837(15), b = 9.892(5), c = 10.446(5) Å, V = 2876(3) Å^3, Z = 4, ρ_{calcd} = 1.724 g cm^{-3}, F_{000} = 1541, Bruker D8 diffractometer, synchrotron radiation, λ = 0.69040 Å, T = 150(2 K, $2\theta_{max}$ = 51.1°, 17391 reflections collected, 5820 unique (R_{int} = 0.1228). Final *GooF* = 1.013, *R1* = 0.0727, *wR2* = 0.1688, *R* indices based on 3398 reflections with $I > 2\sigma(I)$ (refinement on F^2), 506 parameters, 185 restraints. Lp and absorption corrections applied, μ = 1.378 mm^{-1}. Absolute structure parameter = −0.03(4).

Detailed reports on disorder modeling in **2** and **5b** can be found in the Supporting Information (**2:** paragraph III and **5b:** paragraph IV).

Acknowledgements

We thank the Leverhulme Trust for support of J.N.R and the EPSRC for funding under EPSRC/C511794 and for access to the SRS. We thank the Royal Society for a University Research Fellowship (to A.I.C.) and a Wolfson Research Merit Award to M.J.R.

[1] B. F. Hoskins, R. Robson, *J. Am. Chem. Soc.* **1990**, *112*, 1546.
[2] S. R. Batten, R. Robson, *Angew. Chem.* **1998**, *110*, 1558–1595; *Angew. Chem. Int. Ed.* **1998**, *37*, 1460–1494.
[3] M. Eddaoudi, D. B. Moler, H. Li, B. Chen, T. M. Reineke, M. O'Keeffe, O. M. Yaghi, *Acc. Chem. Res.* **2001**, *34*, 319–330.
[4] O. R. Evans, W. Lin, *Acc. Chem. Res.* **2002**, *35*, 511–522.
[5] M. Eddaoudi, J. Kim, N. Rosi, D. Vodak, J. Wachter, M. O'Keeffe, O. M. Yaghi, *Science* **2002**, *295*, 469–472.
[6] X. Zhao, B. Xiao, A. J. Fletcher, K. M. Thomas, D. Bradshaw, M. J. Rosseinsky, *Science* **2004**, *306*, 1012–1015.
[7] O. M. Yaghi, M. O'Keeffe, N. W. Ockwig, H. K. Chae, M. Eddaoudi, J. Kim, *Nature* **2003**, *423*, 705–714.
[8] C. D. Wu, A. Hu, L. Zhang, W. Lin, *J. Am. Chem. Soc.* **2005**, *127*, 8940–8941.
[9] U. Mueller, M. Schubert, F. Teich, H. Puetter, K. Schierle-Arndt, J. Pastre, *J. Mater. Chem.* **2006**, *16*, 626–636.
[10] L. Alaerts, Christine E. A. Kirschhock, M. Maes, Monique A. van der Veen, V. Finsy, A. Depla, Johan A. Martens, Gino V. Baron, Pierre A. Jacobs, Joeri F. M. Denayer, Dirk E. De Vos, *Angew. Chem.* **2007**, *119*, 4371–4375; *Angew. Chem. Int. Ed.* **2007**, *46*, 4293–4297.
[11] L. Alaerts, E. Seguin, H. Poelman, F. Thibault-Starzyk, P. A. Jacobs, D. E. De Vos, *Chem. Eur. J.* **2006**, *12*, 7353–7363.
[12] J. M. Newsam, M. M. J. Treacy, W. T. Koetsier, C. B. De Gruyter, *Proc. R. Soc. London, Ser. A* **1988**, *420*, 375–405.
[13] M. W. Anderson, O. Terasaki, T. Ohsuna, A. Phllippou, S. P. MacKay, A. Ferreira, J. Rocha, S. Lidin, *Nature* **1994**, *367*, 347–351.
[14] T. Ezuhara, K. Endo, Y. Aoyama, *J. Am. Chem. Soc.* **1999**, *121*, 3279–3283.
[15] J. S. Seo, D. Whang, H. Lee, S. I. Jun, J. Oh, Y. J. Jeon, K. Kim, *Nature* **2000**, *404*, 982–986.
[16] C. J. Kepert, T. J. Prior, M. J. Rosseinsky, *J. Am. Chem. Soc.* **2000**, *122*, 5158–5168.
[17] D. N. Dybtsev, A. L. Nuzhdin, H. Chun, K. P. Bryliakov, E. P. Talsi, V. P. Fedin, K. Kim, *Angew. Chem.* **2006**, *118*, 930.
[18] S. Thushari, J. A. K. Cha, H. H. Y. Sung, S. S. Y. Chui, A. L. F. Leung, Y. F. Yen, I. D. Williams, *Chem. Commun.* **2005**, 5515–5517.
[19] E. V. Anokhina, A. J. Jacobson, *J. Am. Chem. Soc.* **2004**, *126*, 3044–3045.
[20] E. V. Anokhina, Y. B. Go, Y. Lee, T. Vogt, A. J. Jacobson, *J. Am. Chem. Soc.* **2006**, *128*, 9957–9962.
[21] R. Vaidhyanathan, D. Bradshaw, J. N. Rebilly, J. P. Barrio, J. A. Gould, N. G. Berry, M. J. Rosseinsky, *Angew. Chem.* **2006**, *118*, 6645–6649; *Angew. Chem. Int. Ed.* **2006**, *45*, 6495–6499.
[22] C. A. Schalley, T. Müller, P. Linnartz, M. Witt, M. Schäfer, A. Lützen, *Chem. Eur. J.* **2002**, *8*, 3538–3551.
[23] K. Biradha, M. Fujita, *J. Chem. Soc. Dalton Trans.* **2000**, 3805–3810.
[24] H. L. Anderson, S. Anderson, J. K. M. Sanders, *J. Chem. Soc. Perkin Trans. 1* **1995**, 2231–2245.
[25] Y. Kubota, K. Biradha, M. Fujita, S. Sakamoto, K. Yamaguchi, *Bull. Chem. Soc. Jpn.* **2002**, *75*, 559–565.
[26] Ni1−N5(Asp) 2.031 versus Ni2−N6(Asp) 2.091, Ni1−O3 2.053 versus Ni2−O7 2.037, Ni1−O1 2.108 versus Ni2−O5 2.019, Ni1−O6 1.972 versus Ni1−O2 1.998, Ni1−O8 2.166 versus Ni2−O4 2.099, Ni1−N1 2.080 versus Ni2−N3 2.078 Å
[27] M. D. Hollingsworth and K. D. M. Harris in *Comprehensive Supramolecular Chemistry, Vol. 6* (Eds.: D. D. McNicol, R. Bishop, F. Toda), Pergamon, Oxford, **1996**, pp. 177–237.
[28] M. Latroche, S. Surble, C. Serre, C. Mellot-Draznieks, P. L. Llewellyn, J. H. Lee, J. S. Chang, H. J. Sung, G. Ferey, *Angew. Chem.* **2006**, *118*, 8407–8411; *Angew. Chem. Int. Ed.* **2006**, *45*, 8227–8231.
[29] C. D. Wood, B. Tan, A. Trewin, H. Niu, D. Bradshaw, M. J. Rosseinsky, Y. Z. Khimyak, N. L. Campbell, R. Kirk, E. Stockel, A. I. Cooper, *Chem. Mater.* **2007**, *19*, 2034–2048.
[30] S. Surble, F. Millange, C. Serre, T. Duren, M. Latroche, S. Bourrelly, P. L. Llewellyn, G. Ferey, *J. Am. Chem. Soc.* **2006**, *128*, 14889–14896.
[31] T. K. Maji, G. Mostafa, R. Matsuda, S. Kitagawa, *J. Am. Chem. Soc.* **2005**, *127*, 17152–17153.
[32] R. Matsuda, R. Kitaura, S. Kitagawa, Y. Kubota, T. C. Kobayashi, S. Horike, M. Takata, *J. Am. Chem. Soc.* **2004**, *126*, 14063–14070.
[33] R. Kitaura, K. Fujimoto, S. I. Noro, M. Kondo, S. Kitagawa, *Angew. Chem.* **2002**, *114*, 141–143; *Angew. Chem. Int. Ed.* **2002**, *41*, 133–135.
[34] X. Wang, L. Liu, A. J. Jacobson, *Angew. Chem.* **2006**, *118*, 6649–6653; *Angew. Chem. Int. Ed.* **2006**, *45*, 6499–6503.
[35] T. K. Maji, K. Uemura, H. C. Chang, R. Matsuda, S. Kitagawa, *Angew. Chem.* **2004**, *116*, 3331–3334; *Angew. Chem. Int. Ed.* **2004**, *43*, 3269–3272.

Received: October 3, 2007
Published online: March 28, 2008

